

Technical note

Improved fluorescence peak integration in the Tekran 2537 for applications with sub-optimal sample loadings

P.C. Swartzendruber^{a,b,*}, D.A. Jaffe^{a,b}, B. Finley^a^aUniversity of Washington, Atmospheric Sciences, 408 ATG Building, Seattle, WA 981195, United States^bUniversity of Washington-Bothell, Interdisciplinary Arts and Sciences, 18115 Campus Way NE, Bothell, WA 98011, USA

ARTICLE INFO

Article history:

Received 26 November 2008

Received in revised form

25 February 2009

Accepted 26 February 2009

Keywords:

Mercury

Methods

CVAFS

Integration

ABSTRACT

The Tekran 2537 is widely used for monitoring atmospheric mercury. Although the instrument was designed for sample volumes in excess of 7.5 L, some recent research applications (e.g. aircraft) have used the instrument with significantly smaller collection times and sample volumes – and therefore smaller Hg loadings per cycle – than for which the instrument was designed. We have noticed a potential for non-linear (low) response in the fluorescence peak integration scheme, and thus the reported concentrations when the Hg loading (per cycle) is less than about 10–15 pg, e.g. at around 1 pg loading, the sensitivity is 25% lower than at 10 pg. We determined that although the atomic fluorescence detector was fundamentally linear down to at least 1 pg, the default peak integration scheme appeared to be optimized for > 10–15 pg cycle⁻¹ and so could introduce non-linearity in smaller peaks (i.e. lower mass loadings). For research applications where achieving maximum accuracy and precision of individual, high-time resolution (<5 min) points is crucial, users can mitigate this behavior by modifying the integration parameters or recording the full fluorescence peak and processing the data offline. Two offline methods of quantifying the peak also improved the precision and thus suggest an improvement in the detection limit is possible.

© 2009 Elsevier Ltd. All rights reserved.

1. Introduction

Mercury is a potent environmental toxin involved in a complex terrestrial–atmospheric–oceanic cycle. It has been the focus of increased research in the last several decades as we have learned that mercury contamination has a global impact on aquatic ecosystems, which ultimately leads to toxic levels of methyl mercury in a variety of important aquatic species. The atmosphere has also been identified as a crucial component of the cycle that distributes mercury globally and leads to contamination in remote regions (Schroeder and Munthe, 1998).

Technical advances in the past 20 years have greatly improved our ability to accurately measure extremely low concentrations of mercury in the environment. The Tekran 2537A Mercury Vapor Analyzer (and now the 2537B) has come into wide use for automated measurement of gas-phase mercury with a time resolution as low as 2.5 min (e.g. Banic et al., 2003; Friedli et al., 2004; Radke et al., 2007; Swartzendruber et al., 2008; Talbot et al., 2007; Talbot et al., 2008).

The method collects Hg on Au cartridges, which is then thermally desorbed and detected by Cold Vapor Atomic Fluorescence Spectroscopy (CVAFS). This method has been widely used for quantification of Hg in water, air, and soils and has generally shown robust performance (e.g. EPA 1631; Fitzgerald and Gill, 1979; Landis et al., 2002). We are not aware of any significant difference in the detection or integration components between the 2537A and 2537B, and so we will make no distinction for the sake of simplicity of the discussion.

The 2537 is routinely calibrated at relatively high mass loadings (>100× the detection limit), but its performance has not been, to the best of our knowledge, evaluated at lower Hg mass loadings (<10 pg cycle⁻¹) typically required for high-time resolution observations.

The non-linear integration response was first noticed during analysis of data collected from our aircraft study of ambient Hg speciation in the Pacific Northwest (Swartzendruber et al., in preparation).

2. Laboratory test

2.1. Test parameters

In order to systematically test for a non-linear integration response, two Tekran 2537B's were synchronized and connected to a common inlet which sampled outdoor air through a 0.2 μm

* Corresponding author. University of Washington, Atmospheric Sciences, 408 ATG Building, Seattle, WA 981195, United States. Tel.: +1 206 543 2480; fax: +1 206 543 0308.

E-mail address: pswartz@atmos.washington.edu (P.C. Swartzendruber).

glass-fiber filter. Both instruments were less than 1-year-old. All method parameters and diagnostic parameters were within nominal values based on the manufacturer's recommendations. Both instruments had sensitivities of $6\text{--}8 \times 10^6$ area units per nanogram of Hg. Their baselines were 0.10–0.20 volts. The baseline deviations (an indicator of system noise) were almost entirely <0.10 mV with an averaging time of 10 s. The Au preconcentration cartridges had only limited use, totaling less than 40 days in clean, low Hg air. The mass flow meters on both instruments were calibrated with a bubble meter immediately before the test and both instruments were leak checked. Before and after this test, multiple span calibrations were conducted on each instrument and an Hg scrubber was connected to the sample line to check the blank levels. Both instruments had consistent calibrations and unquantifiable blanks (<0.1 pg). Also, both instruments were run using identical methods and flow rate, and were found to agree to within 1.0% ($\pm 3.2\%$) at 1.4 ng m^{-3} .

The test was conducted by setting the reference instrument to collect at 1.3 lpm on 5 min cycles while the second instrument collected on 2.5 min cycles at varying flow rates, with the clocks synchronized. In each 5 min cycle of the reference instrument, about 10 pg of Hg was collected, while for the test instrument, each cartridge collected about 4.8, 2.6, 1.8 and 1 pg cycle^{-1} as the flow rate decreased from 1.30 to 0.70, 0.50, and 0.30 slpm. There was minimal cartridge bias ($<3\%$) in both instruments.

2.2. Results

Fig. 1 shows an example peak (about 7000 area units, 1 pg of Hg) from this test where the default 2537 integration algorithm has stopped at point A, which appears to be too early, based simply on visual inspection. The baseline used by the default scheme is indicated by the red-dotted line. Note that this line does not connect to point A because the ending baseline voltage is calculated from the average voltage of the 1-s following the end time (point A). It appears that integration should continue much longer, so point B was selected for the purpose of illustrating an idealized, true ending point, with the correct baseline indicated by the black dashed-dotted line. This figure will be discussed further in Section 3.

Fig. 2 shows the non-linear integration response of the test instrument with mass loadings below 10 pg cycle^{-1} . Each point indicated by the triangles represents the concentration reported by the test instrument as a fraction of the concentration reported by the reference instrument. The open circles represent the original data which has been manually corrected and will be discussed in the following sections.

3. Explanation

3.1. Shape of peak

In order to develop an objective criterion for ending the integration, the tail of a peak with much larger Hg loading (about 250 pg) was investigated to see if any dominating features could be identified. The tail of the peak was found to fit an exponential decay equation

$$y(t) = Ae^{-t/\tau}$$

with $r^2 = 0.9999$ for 15 s (150 points) after the peak maximum. The time constant of the peak decay, $\tau = 2.6$ s, is very similar to what would be expected for a flushing constant for the fluorescence cell ($3.4 \text{ cc cell volume}/1.4 \text{ cc s}^{-1} \text{ flow} = 2.4 \text{ s}$). While the similarity does not necessarily prove that dilution is the only factor controlling

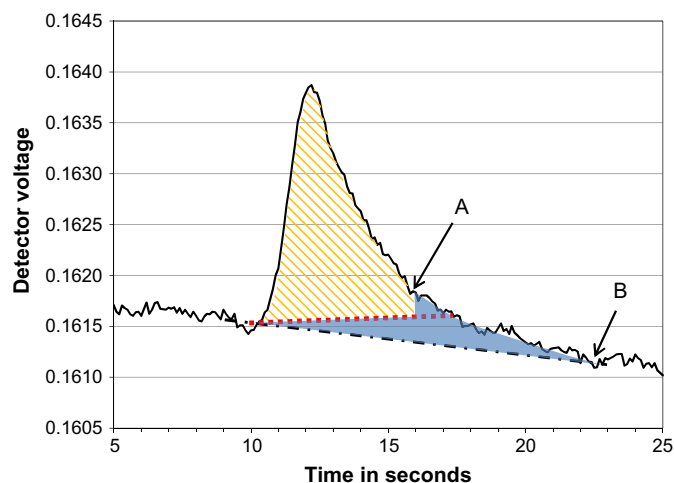


Fig. 1. Example peak from a laboratory test where the 2537 integration stopped at point A, but it appears that it should continue to B. Yellow area (with diagonal hatching) indicates the area reported by the default 2537 integration algorithm, the blue area is the area missed when integration time is corrected. The red-dotted line is the (incorrect) baseline used by the default 2537 algorithm and the dash-dotted line is the true baseline. See Sections 2.2 and 3. (For interpretation of the references to colour in this figure legend, the reader is referred to the web version of this article.)

shape of the tail, this feature clearly dominates. The tail of this peak and other peaks with much smaller Hg masses (including the example peak, Fig. 1) can be superimposed by linear scaling.

The scalability argues that, with a constant volumetric flow rate through the cell, each point of the peak scales with the amount of mercury desorbed and that the shape of the tail is dependent primarily on dilution. This argues that the duration of integration should depend on only the decay time constant (to 5 or 6τ) rather than a signal-to-noise threshold which may be subject to drift. It also provides an objective basis for the observations in Fig. 1 that integration should continue to at least point B. It also supports the reports of, among others, Fitzgerald and Gill (1979), and EPA 1631, that peak height can also be used to quantify the mercury content of a desorption peak.

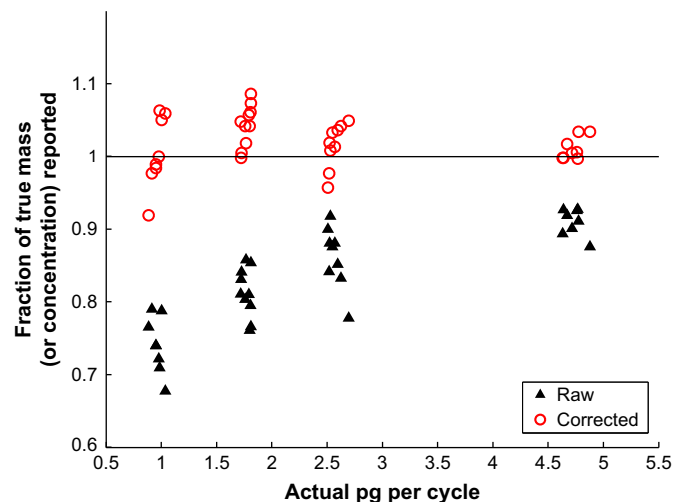


Fig. 2. Scatter plot showing the raw (as triangles) reported concentration of mercury as a fraction of the concentration reported by the reference instrument. The open circles show the corrected original data as a fraction of the reference instrument. The non-linear integration response can be seen as the mass loading per cycle decreases. The corrected data show a linear, unbiased response down to 1 pg cycle^{-1} .

3.2. Limitations of the default integration scheme

According to the User's Manual, the end of the peak is found when the change in the detector output (which has been converted to digital counts at 10 Hz) is less than or equal to V_{Base} , for N_{Base} successive points. Our V_{Base} was 8 and our N_{Base} was 5. In this scheme, the end of the peak is found when the drift (decay) of the signal falls below a threshold, and so will be earlier for peaks with smaller mass. If the threshold is too stringent, the ending times will be on average longer and will have greater variability and the precision could be reduced. On the other hand, if the threshold is not stringent enough, ending times will be earlier and more consistent, but some area will be missed, as in Fig. 1. When the area missed is small relative to the total area (i.e. peaks > 60,000–90,000 area units, or 10–15 pg), the error is negligible. But, because the area that is missed appears to be relatively constant, the percent error will grow non-linearly as the total area decreases. That is, to a first approximation, $error \propto \frac{\text{missed area}}{\text{total area}}$. The uncorrected data fit a theoretical prediction of this effect (not shown).

4. Mitigation

If it is not possible to collect more than 10–15 pg cycle⁻¹, there are two potential routes to mitigating the non-linear integration response. The first approach is to record the full peak dump for every cycle and to quantify the peaks offline with one of three techniques. The second potential solution is to change the integration parameters on the 2537 to increase the integration time. For critical applications, we believe that offline quantification/integration would be the safest approach.

All of the offline techniques have shown good improvement of the non-linearity (e.g. in Fig. 2). Modification of 2537s integration parameters was also successful in bringing the reported response of 1 pg peaks to within about 95% of the reference instrument.

It was also discovered that quantifying the peaks offline by peak height and regression also significantly improved the precision of the method. This can be seen in Fig. 3 and is discussed below.

4.1. Offline peak quantification

Using the raw detector dump from the serial output, we have found three techniques to quantify the mercury content of a peak. In order of increasing complexity, the peaks can be quantified by peak height; integrating peak area for a longer, fixed duration; or regressing the data peak to a calibration peak.

Peak height has been previously reported to produce good results for preconcentration CVAFS and AAS techniques (Fitzgerald and Gill, 1979; EPA 1631). In this technique, the Hg mass of the sample peak is obtained from the ratio of the sample peak height to the calibration peak height. To obtain maximum accuracy and precision, the peak height should be measured from a baseline which is adjusted for drift from before to after the peak (about 5τ after the maximum). This can be accomplished by processing with an offline script, or by reading the output from the peak-table in the serial output.

The peaks can also be quantified with an offline script that integrates for a longer duration. The baseline must also be corrected for drift from before to after the peak.

The third technique for quantifying the peak is to regress the data peak to the appropriate calibration peak. Note that this is simply a logical extension of the peak-height technique. That is, the scaling between the sample peak and the calibration peak is calculated at multiple points. In this technique, chunks of each peak from about 0.5τ before the maximum to about 1.5 – 2.0τ after the maximum are selected. The maxima are aligned and the chunks are shifted forward or backward a step or two (0.1 s each) to the alignment

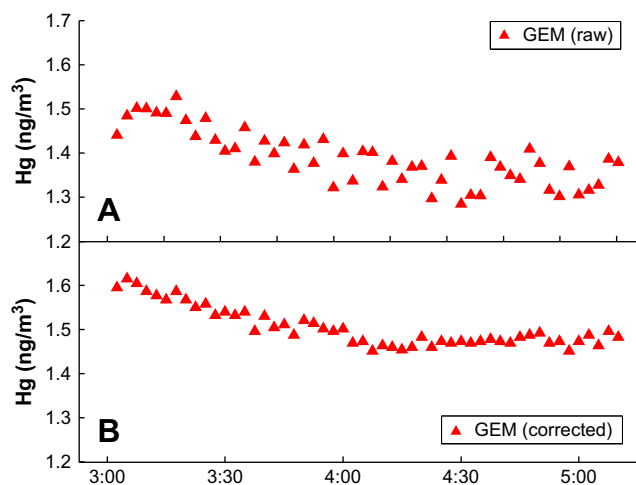


Fig. 3. Example 2.5 min data at 1.0 lpm (about 4 pg cycle⁻¹). Panel A shows the results using the data reported by the 2537 serial output and Panel B shows the data reprocessed offline with the Hg mass quantified by peak height.

which produces the strongest correlation. The regression should only include points which fit the linear relationship, so baseline data should not be included. The slope of the correlation line gives the scaling factor of the data Hg mass to the calibration Hg mass and the precise ending time of the peak is unimportant. E.g., the regression of the peak in Fig. 1 (about 1 pg) to its nearest calibration peak (33.0 pg) has an $r^2 = 0.996$ ($n = 62$).

4.2. Modified integration parameters

The 2537 allows the user to adjust the parameters that control the detection of the end of the peak, N_{Base} and V_{Base} . The non-linear integration response we observed occurred with $N_{Base} = 5$ and $V_{Base} = 8$ (explained previously). We found the best improvement in response by changing these to the most stringent possible, $N_{Base} = 19$ and $V_{Base} = 0$. We replicated the algorithm for detecting the end of the peak, as stated in the manual, and found that the actual detection criteria were less stringent, which suggests a slightly different algorithm was being used.

Modification of the 2537's integration parameters extended the ending of the integration to about 8–9 s, which brought peaks of 1 pg to within about 95% of the reference instrument (which is consistent with integration continuing to about 3τ). While modification of the integration parameters significantly reduced the non-linearity of the integration in our lab test, it still did not consistently bring the integration ending time to 5 – 6τ and thus could still allow for some area to be missed. Nonetheless, we do not know if these changes will be universally successful or could create other problems. We therefore suggest that anyone choosing to modify their integration parameters contact the manufacturer.

5. Results

5.1. Laboratory test

The data collected from the laboratory study is shown in Fig. 2. The peaks were quantified offline by integrating until 17.0 s after the peak maximum. The data from the reference instrument was also reprocessed in the same manner. Reprocessing of the reference instrument data had a negligible effect, but was done to isolate the effects of the lower mass loadings. The non-linear integration response at lower mass loadings is clearly resolved by the revised integration algorithm.

5.2. Aircraft data

Fig. 3 shows an example of 2537 data before a research flight. The instrument sampled at 1.0 lpm on 2.5 min cycles and collected about 4 pg cycle⁻¹. The top panel shows the data based on the 2537 serial output which uses the default integration scheme. The root-mean-squared difference (of successive cycles) using the default integration scheme is 0.050 ng m⁻³. The bottom panel shows the same data when the Hg mass is quantified offline by the peak height technique. (Note that the regression technique yields nearly identical results.) The root-mean-squared difference is reduced to <0.020 ng m⁻³, which implies that the detection limit can be reduced 2-fold by improving the quantification scheme.

Acknowledgements

This research was conducted under funding provide by a NASA grant but has not be subject to any NASA review. The author also wishes acknowledge helpful discussions and advice from F. Schaedlich, D. Schneeberger, and E. Prestbo at Tekran, Inc, and the helpful comments of the anonymous reviewers.

References

- Banic, C.M., Beauchamp, S.T., Tordon, R.J., Schroeder, W.H., Steffen, A., Anlauf, K.A., Wong, H.K.T., 2003. Vertical distribution of gaseous elemental mercury in Canada. *Journal of Geophysical Research* 108 (D9), 4264. doi:10.1029/2002JD002116.
- EPA 1631, August 2002. Revision E: Mercury in Water by Oxidation, Purge and Trap, and Cold Vapor Atomic Fluorescence Spectrometry, US EPA available at: <http://www.epa.gov/waterscience/methods/method/mercury/>.
- Fitzgerald, W.F., Gill, G.A., September, 1979. Subnanogram determination of mercury by two-stage gold amalgamation and gas phase detection applied to atmospheric analysis. *Analytical Chemistry* 51 (11).
- Friedli, H.R., Radke, L.F., Prescott, R., Li, P., Woo, J.-H., Carmichael, G.R., 2004. Mercury in the atmosphere around Japan, Korea, and China as observed during the 2001 ACE-Asia field campaign: measurements, distributions, sources, and implications. *Journal of Geophysical Research* 109, D19S25. doi:10.1029/2003JD004244.
- Landis, M.S., Stevens, R.K., Schaedlich, F., Prestbo, E.M., 2002. Development and characterization of an annular denuder methodology for the measurement of divalent inorganic reactive mercury in the ambient air. *Environmental Science & Technology* 36, 3000–3009.
- Radke, L.F., Friedli, H.R., Heikes, B.G., 2007. Atmospheric mercury over the NE Pacific during spring 2002: gradients, residence time, upper troposphere lower stratosphere loss, and long-range transport. *Journal of Geophysical Research* 112, D19305. doi:10.1029/2005JD005828.
- Schroeder, W.H., Munthe, J., 1998. Atmospheric mercury – an overview. *Atmospheric Environment* 32 (5), 809–822.
- Swartzendruber, P.C., Jaffe, D.A., Finely, B., February 2009. Development and first results of an aircraft based, high time resolution mercury speciation technique, in-preparation.
- Swartzendruber, P.C., Chand, D., Jaffe, D.A., Smith, J., Reidmiller, D., Gratz, L., Keeler, J., Strode, S., Jaegle, L., Talbot, R., 2008. Vertical distribution of mercury, CO, ozone, and aerosol scattering coefficient in the Pacific Northwest during the spring 2006 INTEX-B campaign. *Journal of Geophysical Research* 113, D10305. doi:10.1029/2007JD009579.
- Talbot, R., Mao, H., Scheuer, E., Dibb, J., Avery, M., 2007. Total depletion of Hg⁰ in the upper troposphere–lower stratosphere. *Geophysical Research Letters* 34, L23804. doi:10.1029/2007GL031366.
- Talbot, R., et al., 2008. Factors influencing the large-scale distribution of Hg⁰ in the Mexico City area and over the North Pacific. *Atmospheric Chemistry and Physics* 8, 2103–2114.